

## Broadband optical studies of 1-D and 3-D photonic crystals

Peter T. Rakich<sup>1</sup>, Hideyuki Sotobayashi<sup>2</sup>, Juliet T. Gopinath<sup>1</sup>, Jason W. Sickler<sup>1</sup>, Chee Wei Wong<sup>1</sup>, Steven G. Johnson<sup>1</sup>, Minghao Qi<sup>1</sup>, Eleferios Lidorikis<sup>1</sup>, Henry I. Smith<sup>1</sup>, John D. Joannopoulos<sup>1</sup> and Erich P. Ippen<sup>1</sup>

<sup>1</sup>Research Laboratory of Electronics, Massachusetts Institute of Technology, Cambridge, MA 02139, USA E-mail: rakich@mit.edu

<sup>2</sup>National Institute for Communications and Technology, Tokyo, Japan

### ABSTRACT

Supercontinuum based sources and measurement techniques are developed, enabling optical ultra-broadband studies of nano-scale photonic crystal devices and integrated photonic circuits over 1.2 – 2.0  $\mu\text{m}$  wavelength range. Experiments involving 1-D periodic photonic crystal microcavity waveguides and 3-D periodic photonic crystals with embedded point defects are described. Experimental findings are compared with rigorous electromagnetic simulations.

**Keywords:** supercontinuum, waveguides, photonic crystals, fiber-laser, femtosecond

### 1. INTRODUCTION

High-index contrast photonic crystal waveguides are of interest for an increasing variety of applications. However, the measurements required to understand the basic physical phenomena of photonic crystal devices often present serious experimental challenges. In many cases it is necessary to perform spectral measurements over 50 – 100% of the center frequency of the device (i.e. as much as an octave) in order to understand the bandgap-related phenomena. Additionally, due to the nano-scale dimensions of such devices, high insertion losses and low throughput are typical in a laboratory setting. It is for this reason that high-brightness sources such as tunable lasers are typically used to scan the broad spectral features of photonic crystals. Unfortunately, tunable laser sources spanning the entire 1 – 2  $\mu\text{m}$  spectral range, critical for the study of telecom-centered devices, are not readily available. To facilitate the science and study of photonic crystals and integrated photonic devices, we develop practical femtosecond fiber-laser-based supercontinuum sources (SC) spanning the 1.2 – 2.0  $\mu\text{m}$  wavelength range and broadband SC based measurement techniques. These techniques are then applied to the study of high index contrast photonic crystal devices, enabling a host of new photonic crystal studies. Experiments involving both 1-D periodic photonic crystal microcavity waveguides and 3-D periodic photonic crystals with embedded point defects are described. Experimental findings are compared with rigorous electromagnetic simulations<sup>1,2</sup>.

Earlier applications of SC sources to the study of photonic devices have utilized solid state Ti:Sapphire based SC sources (centered at 800 nm) to the study of two-dimensional photonic crystal slab waveguides with a system utilizing free-space optics<sup>3,4</sup>. In contrast, we develop solid state and all-fiber SC sources centered at telecommunications wavelengths (1.55  $\mu\text{m}$ ) and an all-fiber measurement apparatus for the study of photonic crystals and integrated circuits at telecom wavelengths. To minimize the losses and complexity produced by broadband free-space optics, we focus instead on all-fiber methods for broadband polarization control, and coupling. Additionally, through sensitive detection and careful normalization many of the undesirable aspects of a typical SC source can be mitigated, producing high fidelity measurements over the entire 1.2 – 2.0  $\mu\text{m}$  wavelength range<sup>1,2</sup>.

### 2. Supercontinuum sources and measurement techniques

The SC source developed in this work consists of a length of highly nonlinear dispersion-shifted fiber (HNL-DSF) seeded by a femtosecond stretched-pulse fiber laser, shown in Fig. 1(a). The laser consists of a 55.6 cm length of bismuth oxide-based erbium-doped fiber (Bi-EDF), 1.8 m of low-nonlinearity single-mode fiber (LNL-SMF), two polarization controllers, and a polarizing beam-splitter. The rejection port of the polarizing beam splitter forms the output coupler of the laser, while a bi-directionally pumped length of Bi-EDF fiber serves as the gain medium,

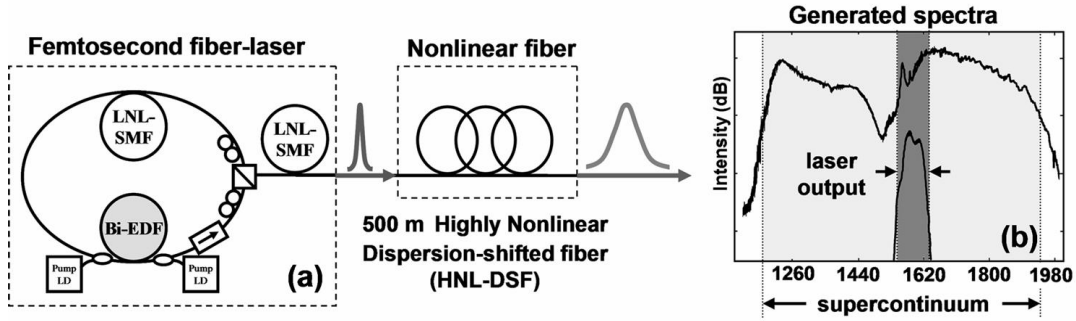


**Figure 1:** (a) Schematic of supercontinuum source, which consists of a femtosecond fiber-laser and a length of highly nonlinear dispersion shifted fiber. (b) Optical power spectrum of the fiber laser output before and after passing through the nonlinear fiber.

providing a broad gain bandwidth and high gain per unit length<sup>5</sup>. To balance the dispersion of the Bi-EDF, and manage the intracavity nonlinearity, 1.8 m of LNL-SMF is included in the laser. Mode-locked operation of the laser was obtained through nonlinear polarization evolution<sup>6</sup>. For pump powers of 350 mW, a 28 mW average output power was obtained with center wavelengths and spectral full-width half maxima of 1571 nm and 58 nm respectively. Through external compression with a 1.8 m segment of LNL-SMF 100 fs pulses were obtained, providing a peak pulse power of ~8.5 kW, which was sufficient for the generation of a broad SC spectrum. Pulses are injected into 500 m of HNL-DSF having a zero-dispersion wavelength of 1565 nm and a nonlinear coefficient of 21 km<sup>-1</sup> W<sup>-1</sup> to generate SC. The laser spectra before and after the HNL-DSF are shown in Fig. 2(b). It should be noted that the supercontinuum light generated by this method is unpolarized when measured at millisecond time scales due to nonlinear polarization evolution produced in the HNL-DSF. Additionally, the nonlinear nature of the SC generation makes the shape of the spectral output very sensitive to changes in laser state<sup>7</sup>.

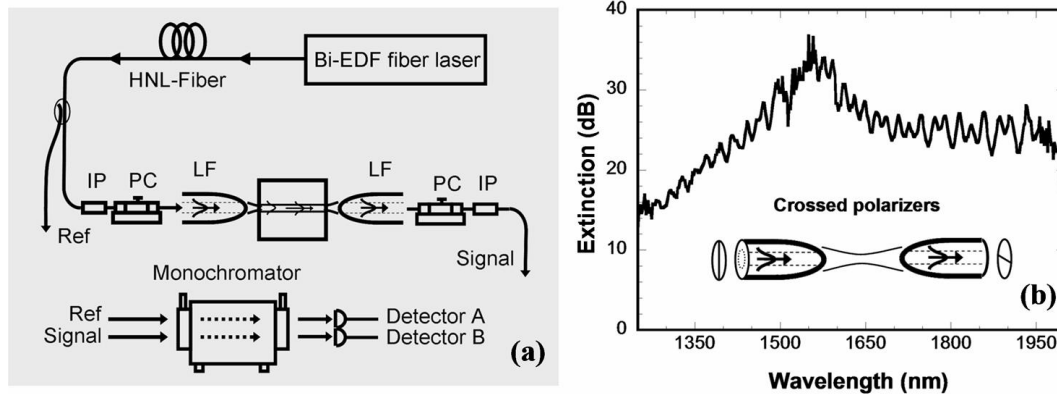


**Figure 2:** (a) A schematic of measurement apparatus. A small fraction of SC light is diverted by a coupler for reference (Ref) measurement while the remainder (Signal) is passed through the waveguide. The signal and reference are then imaged through a monochromator onto identical photo-detectors for real time normalization. (b) Polarization extinction obtained through polarization control method depicted in Fig 2(a).

The SC spectrum generated in the HNL-DSF is coupled into the apparatus shown in Fig. 2(a) for waveguide transmission studies. The unpolarized SC light is first passed through a broadband fiber-optic coupler, splitting the continuum into two ports, signal and reference. The signal is then sent through an inline polarizer and polarization controller, which define the polarization at the input of the waveguide. A lensed fiber is then used to couple the signal into the waveguide. A second lensed fiber collects the waveguide output that is sent through a polarization controller and inline polarizer for polarization analysis. The signal and reference are then imaged through a monochromator onto two identical photodetectors, for real-time normalization of the SC fluctuations and spectral changes. Detection is performed with Peltier cooled IR-enhanced InGaAs photodiodes and lock-in amplifiers to achieve low noise measurements (with a noise equivalent power of 28 fW/√Hz) and enable rapid scans (less than one minute) with as little as 4 mW of SC light.

Polarization control of the light launched into the waveguide and polarization analysis of the light collected from the guide were performed with use of broadband inline polarizers and strain-type polarization controllers as depicted in Fig 2(a). As can be seen in Fig. 2(b), this provides greater than 20 dB of polarization extinction over most of the spectral range of the SC source. However, critical to broadband performance is (1) the type of inline polarizer used, and (2) minimization of polarization mode dispersion (PMD) which follows the polarizer. Laminated inline polarizers of the type described in reference [8] were used, providing high extinction and low insertion losses over the entire 1 – 2  $\mu\text{m}$  wavelength range. PMD was managed by minimizing the length of fiber between the polarizer and lensed fiber, as well as any bending experienced by the fiber. For the measurement shown in Fig 2(b), fiber lengths were kept below 30 cm. Additionally, through a slight change in the state of the polarization controller >25 dB contrast can be achieved at any wavelength in the 1.2 – 2.0  $\mu\text{m}$  range, enabling higher polarization extinction through more than one wavelength scan if needed.

### 3. Studies of 1-D periodic photonic crystal with a defect

This measurement method was applied to the study of a number of HIC devices, however, in this paper we will examine a 1-D photonic bandgap microcavity and 3-D photonic crystal with point defects<sup>2</sup>. The 1-D photonic crystal microcavity, which has been studied extensively over the past several years, consists of a silicon strip on top of an oxide layer, forming a waveguide with a single TE-like mode over much of the 1 – 2  $\mu\text{m}$  wavelength range<sup>9,10</sup>. A 1-D periodic photonic crystal is patterned in the waveguide by etching a periodic array of holes through the silicon strip. The photonic crystal defect is then defined in the photonic crystal by increasing one hole spacing from  $a$  (the lattice constant) to  $a_d$  (the defect length). A device schematic and scanning electron micrograph (SEM) are shown in Fig. 3(b).

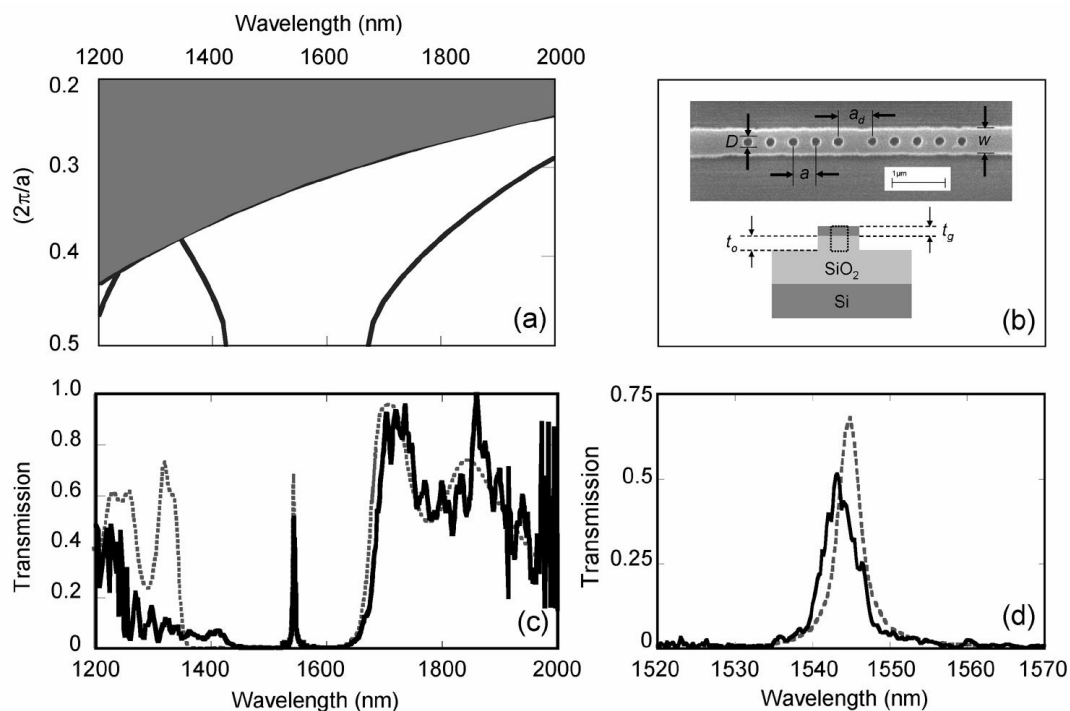


**Figure 3:** (a) Band diagram (TE-like bands only) based on SEM measurements of device. Grey region indicates states above the light line. (b) SEM of microcavity (top) and cross-section of waveguide (bottom). Device parameters extracted from SEM are  $a = 424$  nm,  $a_d = 649$  nm,  $w = 494$  nm,  $t_g = 195$  nm,  $t_0 = 350$  nm, and  $D = 179$  nm. (c) A transmission measurement (solid) and simulated transmission (dashed) of photonic crystal microcavity (TE polarization). The transmission measurement is normalized to that of a similar waveguide without etched holes. (d) High resolution (0.1 nm) measurement (solid) and simulation (dashed) of the microcavity resonance.

For comparison with experiments, simulations of the device band structure and power transmission were performed based on the parameters extracted from SEM measurements<sup>11,12</sup>. Results of the band-structure computations for the TE-like mode can be seen in Fig 3(a) while the dashed curve of Fig 3(c) shows the simulated power transmission of

the TE-like mode. In comparing the two, we see that the photonic bandgap results in a stop-band spanning approximately 400 nm, while the photonic crystal defect results in a sharp resonance within the stop-band. It is apparent from the theoretical transmission that even a photonic crystal device as elementary as this requires very broadband characterization. Complete study of the photonic bandgap requires a measurement window which is greater than 500 nm. Additionally, for the study of bandgap related phenomena, larger bandwidths are often desirable.

Due to high insertion losses (typically ~15 dB) at the input and output facets of nanometer-scale waveguides of this type, and the large attenuation obtained within the bandgap (~30 dB), high brightness sources such as tunable lasers are typically employed in laboratory studies. However, tunable laser sources are not widely available over such broad bandwidths in the NIR, making supercontinuum sources and techniques indispensable for broadband studies in at these wavelengths.

Through the supercontinuum-based techniques described above, transmission measurements of the 1-D photonic crystal were obtainable over ~800 nm bandwidths. Superposed with the theoretical transmission (dash) of Fig. 3(c) is the measured transmission spectrum (solid) obtained with the apparatus shown in Fig. 2(a). It is important to note, however, that normalization was crucial for direct comparison of the experimental trace with theory. Broadband transmission through a waveguide device such as this is typically distorted by wavelength dependent coupling and waveguide propagation losses, which aren't of interest when examining the photonic crystal behaviour. However, these unwanted spectral features can be removed through careful normalization of the photonic crystal device transmission to an identical waveguide without a photonic crystal (a reference waveguide). Normalization to a reference waveguide is also crucial to the removal of any wavelength dependence of the apparatus.

Before a detailed comparison of the theoretical spectrum with experiment, it should be noted that, although SEM measurements yield a lattice constant of  $a = 424 \text{ nm} \pm 5\%$ , it was found that simulations demonstrate best agreement when using  $a = 410 \text{ nm}$ . This adjustment is within the experimental uncertainty; no other parameters were adjusted. In comparing the curves of Fig. 3(c), remarkable agreement is seen between the salient features of both experiment and theory for wavelengths between 1400 – 2000 nm. A 265 nm stop-band is clearly visible in the experiment from approximately 1425 – 1690 nm, and a sharp cavity resonance falls close to theory. Closer examination of the cavity resonance is also made through a high-resolution scan (0.1 nm resolution) shown in Fig. 3(d), revealing a sharp microcavity resonance at 1542 nm. On resonance, efficient power coupling through the photonic crystal is observed, with approximately 52% transmission. This is in reasonable agreement with the simulated transmission efficiency of 68%. However, for wavelengths below 1400 nm the onset of a higher order waveguide mode complicates the device behaviour, resulting in some discrepancy between experiment and theory. Nevertheless, this method clearly resolves the photonic bandgap and the defect resonance, demonstrating a remarkable wavelength range for the study of photonic crystals in the NIR.

#### **4. 3-D periodic photonic crystal with point defects**

A similar supercontinuum based technique was applied to the study of a 3D photonic crystal with embedded point defects, enabling high spatial resolution studies (with a 2.5  $\mu\text{m}$  spot size) of a small number of defects which were randomly distributed within the PhC. An SEM of the 3-D PhC under study can be seen in Fig. 4(c), which was fabricated in Silicon through a layer-by layer process utilizing several successive e-beam lithography steps. This 3-D photonic crystal exhibits a 21% complete photonic bandgap centered at telecom wavelengths. The details of this fabrication process can be found in [1]. The fabricated structure consists of alternating layers of two complementary 2-D photonic crystal slabs, one layer of dielectric rods and another of air holes in a dielectric slab. Embedded within the PhC are randomly distributed defects, each consisting of a completely filled air hole. Defects of this type produce a spatially localized photonic crystal mode, having numerous resonant states within the photonic bandgap, which can couple to external radiation modes. These defects are dispersed within the photonic crystal with a density of 15%.

Despite the remarkable fabrication quality, homogeneities in the environment of these point defects is unavoidable, resulting in inhomogeneous broadening of defect states throughout the PhC. For this reason it was necessary to probe very small areas of the PhC to resolve the energy spectrum of individual defect cavities. Spectroscopic studies of these defects over small areas proved difficult with thermal white light sources due to their low brightness. However, SC based measurement techniques proved valuable in yielding high fidelity measurements of a small number of nano-scale PhC defects, allowing the energy spectrum of individual defects to be fully resolved.

Through Optical study of the 3-D PhC defect states, supercontinuum-based confocal reflection and transmission measurements were employed. The single spatial-mode output of the fiber-based supercontinuum source makes it relatively easy to form small spot sizes with use of a lensed fiber, enabling the study of a small number of defects embedded within the PhC. An average of 3 PhC defects could be studied with use of a single-mode supercontinuum source, when the supercontinuum light is focused to a Gaussian spot size of  $2.5 \mu\text{m}$  within the PhC volume. The supercontinuum source used in these studies consisted of a Ti:Sapphire pumped optical parametric oscillator (OPO) which was used to seed the SC generation in a highly nonlinear fiber, generating SC spanning  $1.2 - 2.0 \mu\text{m}$ . Further details about the SC source are described in *Rakich et al.* [13]. A reference channel was used to normalize for any spectral or temporal variations, in a way similar to that described above. However, unpolarized SC light was sufficient to observe the defect resonances, making polarization control unnecessary in these experiments.

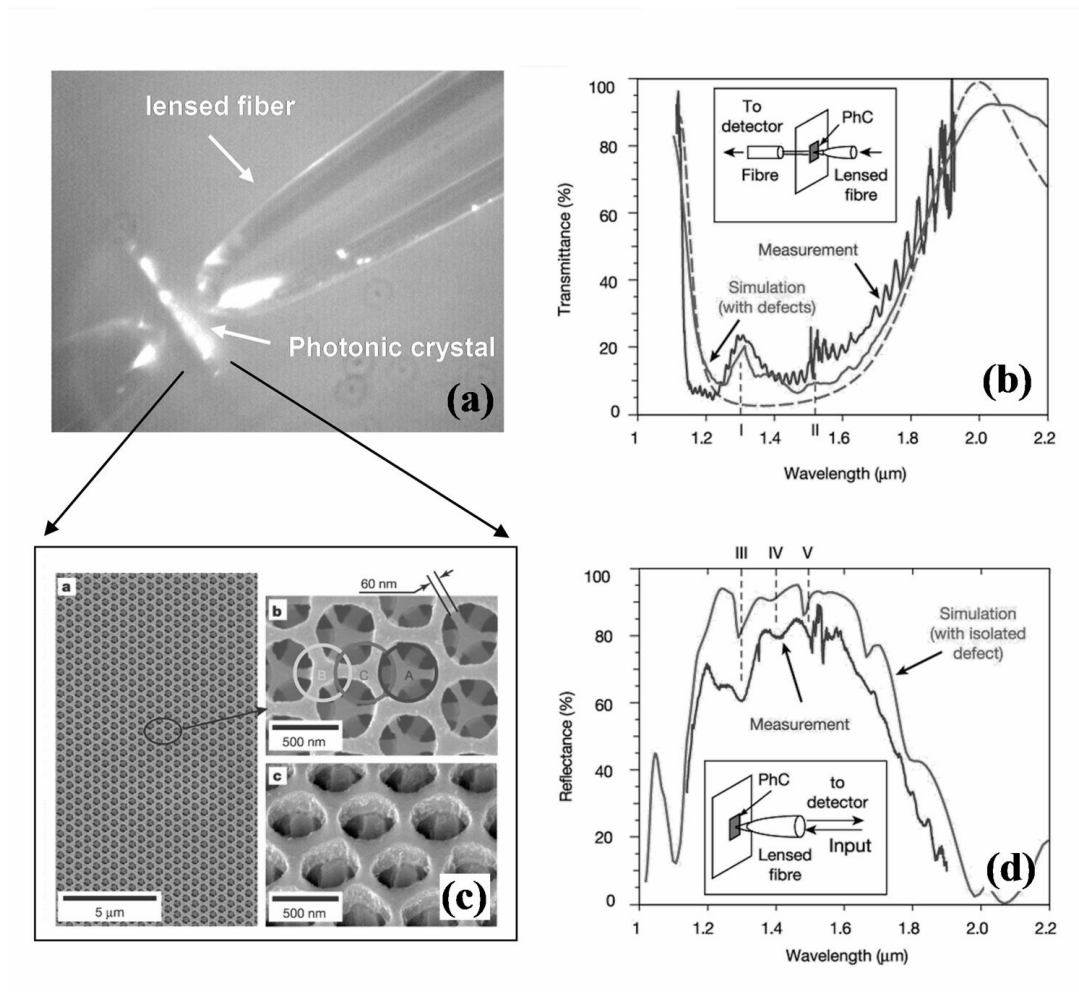


**Figure 4:** (a) photo of lensed fiber and photonic crystal 3D PhC device under test (b) Theoretical (aqua) and experimental (red) transmission spectra of 3D PhC with defects. Theoretical transmission of PhC without defect states (green dash). (c) SEM of 3D fabricated SEBL (d) Theoretical (aqua) and experimental (red) reflection spectra of 3D PhC with point defects.

Spatially localized reflection measurements, taken by this method, were performed at numerous positions on the photonic crystal. Some characteristic reflection and transmission measurements can be seen in Figs. 4(b) and (d) along with the corresponding theoretical transmission and reflection spectra computed through 3D FDTD computations. The experimental geometry for the transmission measurement is depicted in the inset of Fig. 4(a). Here a lensed fiber forms a  $2.5 \mu\text{m}$  Gaussian spot size on the PhC, while a flat-cleaved single mode fiber optic was used to collect the light transmitted through the PhC over a narrow range of transverse wave-vectors (corresponding to  $\sim 1^\circ$  half angle). The PhC transmission spectrum was then normalized to a similar measurement through the same

substrate, without the PhC in the path. We can see that the bandgap of the PhC is clearly resolved along with two peaks in the transmission spectrum (denoted by I & II in Fig. 4(b)), corresponding to resonant transmission through the multi-mode point defects. This can be seen by comparing the theoretical (aqua) and experimental (red) transmission spectra. Such peaks in transmission are not found in simulations of the structure without defect states (green), clearly indicating that these spectral features result from resonant transfer of power through the defect modes. The spectral signatures of the defect modes are somewhat less pronounced for the transmission spectrum, however, more striking features resulting from the defect states are observed as dips in the reflection spectrum. This is because the reflection measurement probes a large transverse wave-vector range (corresponding to a 15.5° half angle), which is more suitable for coupling to localized defect states which tend to radiate over large solid angles. A detailed comparison of the experimental (red) and theoretical (aqua) reflection spectra can be made from Fig 4(d). Three dips are observable in the reflection spectrum at approximately 1.4  $\mu\text{m}$ , 1.5  $\mu\text{m}$  and 1.6  $\mu\text{m}$  wavelengths (denoted by III, IV & V in Fig. 4(d)), which result from resonant coupling to localized defect states within the PhC. The observed stop band and the positions of the defect resonances are in remarkable agreement with the simulated reflection spectrum. It should also be noted that all parameters used to simulate the transmission spectra shown below were extracted from SEMs of the device, and no free parameters were used.

In conclusion, newly developed supercontinuum sources and techniques provide a practical means of studying photonic devices over broad wavelength ranges in the NIR, enabling a host of new studies involving both 1-D periodic photonic crystal microcavities and 3-D periodic photonic crystals. An all-fiber apparatus enables very practical and low-loss means of utilizing supercontinuum sources over the 1.2 – 2.0  $\mu\text{m}$  wavelength range for photonic crystal studies. Additionally, through sensitive detection and careful normalization many of the undesirable aspects of a typical SC source can be mitigated, producing high fidelity measurements of nano-scale photonic devices over the entire 1.2 – 2.0  $\mu\text{m}$  wavelength range.

#### ACKNOWLEDGEMENTS

This work was supported at MIT in part by the Materials Research Science and Engineering Center program of the National Science Foundation and by the U.S. Air Force Office of Scientific Research.

#### REFERENCES

1. Qi, M. H. *et al.* A three-dimensional optical photonic crystal with designed point defects. *Nature* **429**, 538-542 (2004).
2. Rakich, P. T. *et al.* Nano-scale photonic crystal microcavity characterization with an all-fiber based 1.2-2.0  $\mu\text{m}$  supercontinuum. *Opt. Express* **13**, 821-825 (2005).
3. Neal, R. T. *et al.* Ultrabroadband transmission measurements on waveguides of silicon-rich silicon dioxide. *Appl. Phys. Lett.* **83**, 4598-4600 (2003).
4. Netti, M. C. *et al.* Separation of photonic crystal waveguides modes using femtosecond time-of-flight. *Appl. Phys. Lett.* **81**, 3927-3929 (2002).
5. Kuroiwa, Y. *et al.* in *OFC 2001. Optical Fiber Communication Conference and Exhibition. Technical Digest, 17-22 March 2001* 5-1 (Opt. Soc. America, Anaheim, CA, USA, 2001).
6. Haus, H. A., Tamura, K., Nelson, L. E. & Ippen, E. P. Stretched-Pulse Additive-Pulse Mode-Locking in Fiber Ring Lasers - Theory and Experiment. *IEEE J. Quantum Electron.* **31**, 591-598 (1995).
7. Newbury, N. R., Washburn, B. R., Corwin, K. L. & Windeler, R. S. Noise amplification during supercontinuum generation in microstructure fiber. *Opt. Lett.* **28**, 944-946 (2003).
8. Shiraishi, K., Hatakeyama, H., Matsumoto, H. & Matsumura, K. Laminated polarizers exhibiting high performance over a wide range of wavelength. *J. Lightwave Technol.* **15**, 1042-1050 (1997).
9. Foresi, J. S. *et al.* Photonic-bandgap microcavities in optical waveguides. *Nature* **390**, 143-145 (1997).
10. Wong, C. W. *et al.* Strain-tunable silicon photonic band gap microcavities in optical waveguides. *Appl. Phys. Lett.* **84**, 1242-1244 (2004).
11. Johnson, S. G. & Joannopoulos, J. D. Block-iterative frequency-domain methods for Maxwell's equations in a planewave basis. *Opt. Express* **8**, 173-190 (2001).
12. Kunz, K. S. & Luebbers, R. J. The finite-difference time-domain method for electromagnetics. (CRC Press: Boca Raton, 1993).
13. Rakich, P. T. *et al.* in *2004 IEEE LEOS Annual Meeting Conference Proceedings, LEOS 2004, Nov 7-11 2004* 813-814 (Institute of Electrical and Electronics Engineers Inc., Piscataway, NJ 08855-1331, United States, Rio Grande, Puerto Rico, 2004).